Astron. Astrophys. 356, L41–L44 (2000)

ASTRONOMY AND ASTROPHYSICS

LETTER

Letter to the Editor

DG Tau: A shocking jet⋆

C. Lavalley-Fouquet[1], **S. Cabrit**[2], **and C. Dougados**[1,3]

[1] Laboratoire d'Astrophysique de l'Observatoire de Grenoble, B.P. 53, 38041 Grenoble Cedex, France
[2] Observatoire de Paris, DEMIRM, UMR 8540 du CNRS, 61 Avenue de l'Observatoire, 75014 Paris, France
[3] Canada-France-Hawaii Telescope Corporation, PO Box 1597, Kamuela HI 96743, USA

Received 15 February 2000 / Accepted 26 February 2000

Abstract. We present spectro-imaging observations of DG Tau at 0.5″ resolution obtained with OASIS in [O I]λ6300, Hα, [N II]λ6583, and [S II]$\lambda\lambda$6716,6731. The fast jet core appears wiggling and surrounded by a slower moving flow or cavity. Line ratios are compared with available predictions for heating mechanisms in T Tauri jets (shocks, ambipolar diffusion, turbulent mixing-layers). Shocks with speeds 50-100 km s^{-1} increasing with flow velocity, and preshock densities 10^5-10^3 cm^{-3} decreasing away from the star, are best able to reproduce the high level of excitation for velocities $>$ 100 km s^{-1}.

Key words: shock waves – stars: individual: – stars: pre-main sequence – ISM: jets and outflows

1. Introduction

High-velocity forbidden line emission from T Tauri stars (TTS) has been shown to arise in "microjets" detected out to a few 100 AU (Solf & Böhm 1993, hereafter SB93; Hirth et al. 1997) with typical transverse widths $\sim$ 60-100 AU (Dougados et al. 2000). A long-lasting open issue is how the jet remains hot enough to emit at these distances. Given its small launching radius ($\leq$ 0.1-1 AU for high-velocity gas; e.g. Cabrit et al. 1999), dramatic adiabatic cooling should occur in the wind expansion region and extended forbidden line emission should not be detectable (Hartmann & Raymond 1989). Several heating mechanisms have been invoked for TTS microjets: (1) shocks against the disk, the environment, or within the jet itself (Hartmann & Raymond 1989; Hartigan, Edwards & Gandhour 1995, hereafter HEG95; Gómez de Castro & Pudritz 1993), (2) ambipolar-diffusion heating (Safier 1993a,b; Garcia et al. 2000), (3) turbulent dissipation in a viscous mixing-layer (Raymond et al. 1994; Binette et al. 1999), (4) compression by jet instabilities (Bacciotti, Chiuderi & Oliva 1995), but no clear conclusion has been reached so far.

In this Letter, we reconsider this problem using sub-arcsecond spectro-imaging data of DG Tau in [O I]λ6300, Hα, [N II]λ6583, and [S II]$\lambda\lambda$6716,6731, that extend our earlier study (Lavalley et al. 1997, hereafter Paper I) and provide line ratios with higher spatial resolution than achieved so far in this and other TTS (Mundt et al. 1987; Hirth et al. 1997). We show that shock-heating is strongly favored in the DG Tau microjet down to 0.5″ from the star and discuss implications for the jet structure.

2. Observations and data reduction

Observations were carried out at CFHT on Jan. 23-26, 1998 with the integral field spectrograph OASIS using a spatial sampling of 0.16″/lens. Despite a seeing $\geq$ 1″, adaptive optics correction provided a final resolution of 0.5″ (FWHM). Two spectral configurations were observed, covering 6209-6549Å and 6492-6838Å, with a velocity resolution of $\simeq$ 90 km s^{-1} and on source integration times of 2300 and 7310 sec respectively. Following standard OASIS reduction (see Bacon et al. 2000), spectrophotometric calibration was achieved with the standard star HD 44811. The estimated uncertainty is $<$ 10%. At each position, the photospheric Li I λ6707 line (scaled by the continuum PSF) was subtracted from the blue wing of [S II]λ6716. The line profile of the spatially unresolved Hα component at the star position, believed to arise in magnetospheric accretion columns, was similarly subtracted to reveal any extended Hα jet emission. We adopt hereafter the notation [O I] $\equiv$ [O I]λ6300, [N II] $\equiv$ [N II]λ6583; [S II] $\equiv$ [S II]λ6731.

3. Jet morphology and kinematics

The jet morphology and kinematics are illustrated in Figs. 1-2. Emission in Fig. 1 is separated into three velocity intervals: HV = [-400,-250] km s^{-1}, IV = [-250,-100] km s^{-1}, LV = [-100,10] km s^{-1}. Within $\simeq$ 1.3″ of the star, all three intervals are dominated by a bright jet body, showing a steep velocity increase with distance first noted by SB93 (see Fig. 2). A strong emission peak, previously undetected, is observed at 0.93″ from the star, where velocity reaches its maximum (-350 km s^{-1} in

Send offprint requests to: sylvie.cabrit@obspm.fr

⋆ Based on observations collected at the Canada-France-Hawaii Telescope (CFHT), operated by the National Research Council of Canada, the Centre National de la Recherche Scientifique, and University of Hawaii.

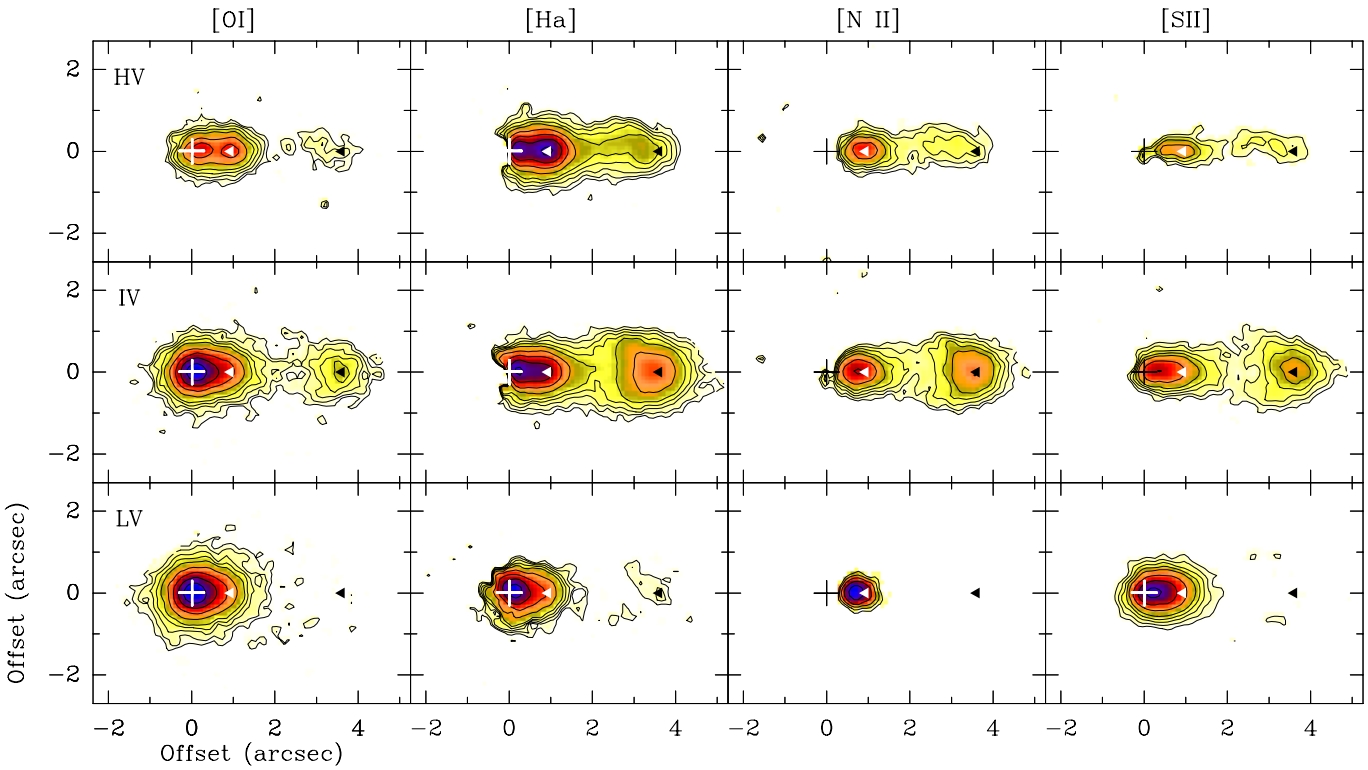

Fig. 1. Continuum-subtracted maps of the DG Tau microjet in [O I]λ6300, Hα, [N II]λ6583, and [S II]λ6731; Velocity ranges are HV [-400,-250] km s^{-1} (top row), IV [-250,-100] km s^{-1} (middle row), and LV [-100,10] km s^{-1} (bottom row). Contours in units of 10^{-18} W m^{-2} arcsec^{-2} start at 2.4, increasing by factors $2^{1/2}$ for the next 4 levels and by factors of 2 for the following ones. A cross indicates the continuum position (0,0); filled triangles mark the high-velocity peak (0.93″) and bowshock apex (3.6″).[1]

[O I]). The HV is barely resolved (FWHM$\leq$ 0.6″), while the IV and LV have a width increasing with distance up to 0.7″ and 0.9″ (FWHM) at 1″.

Beyond 1.3″, the flow structure changes notably: jet velocity drops to -280 km s^{-1} in both [O I] and [N II], and surface brightness diminishes strongly. The transverse widths increase, and the 3 velocity intervals take more distinct morphologies: The HV traces a collimated, slightly wiggling jet beam (FWHM $\simeq$ 0.8-1.0″); The IV traces a broader flow or "cavity" (FWHM $\simeq$ 1-1.7″) in the wake of a bright bowshaped knot at 3.6″, previously identified in Paper I (we derive a proper motion of 0.3″/yr, in complete agreement with Dougados et al. 2000); LV emission is dominated by a faint component emitting mostly in [O I] with surface brightness of $\simeq 3 \times 10^{-18}$ W m^{-2} arcsec^{-2}, and extending at least $\pm$ 2″ from the jet axis. This emission does not appear in Fig. 1 but is detected after some spatial averaging, e.g. in Fig. 2, and probably corresponds to the [O I] 'halo' identified in Paper I.

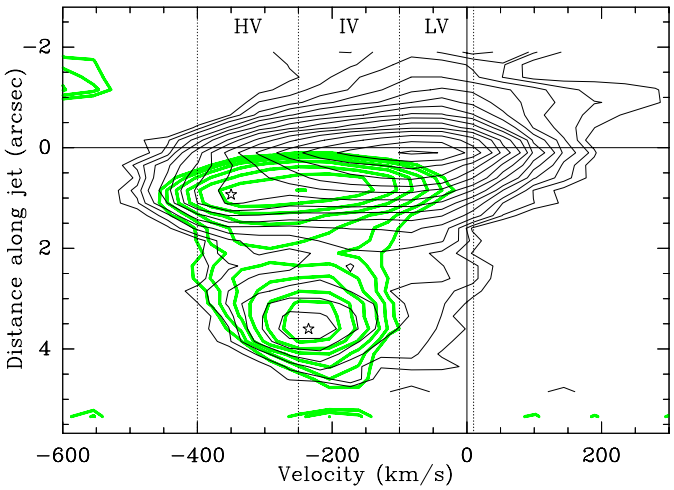

Fig. 2. Position-velocity map along the jet in [N II] (thick grey) and [O I] (thin black), integrated over a 2″ wide 'slit' and sampled every 0.25″. Between 1.5″ and 3″, emission is dominated by the HV jet in [N II], and by the IV "cavity" in [O I]. Contours increase by factors of $2^{1/2}$. Stars mark the high-velocity peak and the bowshock apex.

4. Line excitation mechanism

Since subtraction of the central Hα profile introduces a greater uncertainty in Hα fluxes, we will base our analysis on the following three forbidden line ratio diagnostics (see e.g. Bacciotti & Eislöffel 1999, hereafter BE99): (1) [S II]λ6716/λ6731 is a well-known decreasing function of the electronic density n_e until $n_e \geq n_{cr} \sim 2 \times 10^4$ cm^{-3}, the critical density of [S II]; (2) [N II]/[O I] increases with the electronic fraction $x_e = n_e/n$(H);

[1] Colored version of Fig. 1 is available electronically with the Online publication at http://link.springer.de/link/service/journals/00230/.

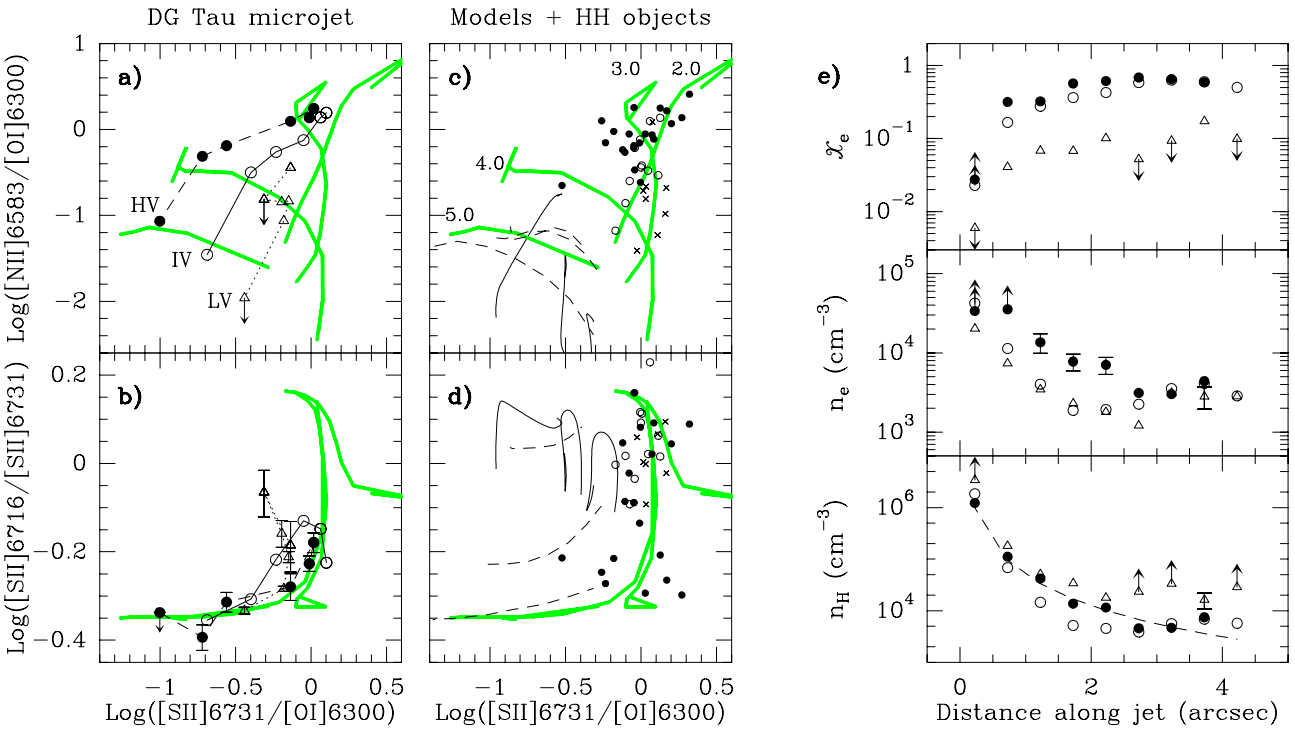

Fig. 3. a–b: Line ratios along the DG Tau jet in the HV, IV, and LV velocity intervals. Points are connected with increasing distance from the star (d= $0.2'', 0.7'', 1.2'', 1.7'', 2.7''$, and $3.7''$), d increasing with [N II]/[O I]. **c–d**: *Grey curves:* planar shocks with B_o = 100μG and $\log_{10}(n_o)$ labelled in **c**. Shock speed increases with [N II]/[O I] along each curve, from 15 to 100km s^{-1} (30 to 80km s^{-1} for n_o = 10^5cm^{-3}); *Dashed lines:* viscous mixing-layers with neutral boundaries ($T = 1000\ K$) of density $n_{env} = 10^5, 10^6, 10^7$ cm^{-3} (top to bottom); layer thickness increases with [S II]/[O I]; *Thin curves:* ambipolar diffusion-heated disk wind with accretion rates of $10^{-8}, 10^{-6}, 10^{-5}$ M$_\odot$ yr^{-1} (left to right), convolved with an 80 AU beam. Distance from star increases with [N II]/[O I] along each curve, from 0 to 600 AU ($4''$); *Symbols:* HH objects of high (filled circles), middle (open circles) and low (crosses) excitation from Raga et al. (1996). **e**: Derived x_e, n_e and n_H along the DG Tau jet for the 3 velocity intervals, same symbols as in **a–b**. Error bars smaller than symbols are not drawn. The dashed curve shows a $1/d^2$ law

(3) [S II]/[O I] decreases with increasing electronic temperature T_e, and with increasing n_e for densities above n_{cr}.

4.1. Observed line ratios and excitation parameters

Figs. 3a-b plot the evolution of line ratios along the DG Tau jet in the 3 velocity intervals defined in Sect. 3 (using a $2''$ wide 'slit' sampled every $0.5''$ along the jet). Fig. 3e plots the inferred x_e, n_e, and n_H= n_e/x_e evaluated with the diagnostic procedure proposed by BE99. Values of T_e (not plotted) show no clear systematic trend with distance and/or velocity[2]. We find that n_e is $> n_{cr}$ within $0.5''$ from the star, then rapidly falls off with distance, except for a local increase at the bowshaped knot ($3.6''$). In contrast, x_e, directly reflecting the variation in [N II]/[O I], increases with distance at all velocities, from $\simeq$0.04-0.2 at $0.7''$ up to $\simeq$ 0.1-0.6 at $3''$. Finally, at a given position, we find that both x_e ([N II]/[O I]) and n_e increase with flow velocity. The resulting n_H decrease is close to a $1/d^2$ law (see Fig. 3e). Note that n_e and n_H for the LV may be overestimated beyond $1.7''$, the IV contributing significantly to the [S II] flux in the LV interval at our limited velocity resolution.

The increase of x_e away from the star, while opposite to the trend observed at larger distances ($d > 1000$ AU) in most HH jets (BE99), is strikingly similar to results recently obtained in the Th 28 and HH 30 jets within 500 AU of the central source (BE99; Bacciotti et al. 1999), and may share a common origin.

4.2. Comparison with heating mechanisms

Figs. 3c-d plot line ratios for 3 models with available quantitative predictions: planar shocks (Hartigan, Morse, Raymond 1994; HEG95), viscous mixing layers with neutral boundaries (Binette et al. 1999), and ambipolar-diffusion heated disk winds (Garcia et al. 2000). Line ratios in HH objects, from the compilation of Raga et al. (1996), are also shown for comparison.

All shock models are found to follow a well-defined 'shock sequence' in the [S II]6716/6731 versus [S II]/[O I] diagram (Fig. 3d), not affected by the strength of the magnetic field, while in the [N II]/[O I] versus [S II]/[O I] diagram, curves for differing pre-shock densities n_o are clearly separated. HH objects closely follow shock sequences with n_o of 10^2-10^3 cm^{-3}, as expected. Being hotter (T $\sim$ 1-3 10^4 K) and of low ionisation, due to turbulent diffusion of ionized species out of the layer (see Binette

[2] We caution that (x_e,T_e) calculated with this procedure could be too large by up to a factor 2 in regions with high excitation and strong spatial gradients (e.g. high-velocity shocks). However, relative variations are preserved.

et al. 1999) mixing layers separate well from planar shocks in these graphs at all but the highest densities ($n_{env} \geq 10^7$ cm^{-3}). Ambipolar diffusion in disk winds establishes similar high temperatures, with low ionization fractions < 0.1 (Safier 1993a; Garcia et al. 2000), leading again to a clear separation from the shock model curves. Predicted ratios are plotted in Fig. 3 for a representative disk wind structure (cf. 'Model 1' parameters in Cabrit et al. 1999).

Comparison with Fig. 3a-b shows that beyond 0.2″, the high [N II]/[O I] ratio in DG Tau excludes both mixing-layers with neutral boundaries and current models of MHD disk winds heated by ambipolar diffusion. Modified models (e.g. mixing-layers with ionized boundaries, ambipolar diffusion in X-winds) might come in closer agreement to observations, but predictions are not yet available. In constrast, shocks readily appear as a very promising mechanism: Observed line ratios in DG Tau cluster around the 'shock sequence' in Fig. 3b and, in both line ratio diagrams, the HV and IV at $d \geq 1.2''$ occupy the same region as the densest high-excitation HH objects. The LV component beyond 1.7 ″ is the only point to significantly deviate from the 'shock sequence'. However, line ratios for this faint component may be contaminated by the IV at our low spectral resolution as well as by residual night sky [O I], preventing to derive firm conclusions on its excitation mechanism.

If shocks are indeed the dominant excitation mechanism in the HV and IV ranges at $d > 0.5''$, comparison with planar shocks would indicate shock speeds V_s in the range 70-100 km s^{-1} for the HV, 50-60 km s^{-1} for the IV (except 70-100km s^{-1} at the bow apex), pre-shock densities $n_{\rm o}$ decreasing away from the star (from 10^5cm^{-3} at 0.22″ to 10^3cm^{-3} at 3.5″) and magnetic fields of 30-100 μG. The decreasing shock speed at lower flow velocity appears reasonable for a broad range of shock geometries, and might explain why integrated forbidden line ratios in DG Tau at $|V| > 60$ km s^{-1} were not reproduced by a single shock (HEG95). Surface brightnesses are also consistent with the above shock parameters if A_V towards the jet is small.

5. Discussion

The hypothesis of shock excitation is further supported by the following morphological and kinematical characteristics of the DG Tau jet: (1) the curved shape with extended faint wings of the outer knot (Fig. 1), and the velocity gradient from the knot apex to the wings (Paper I), are strongly suggestive of a bowshock; (2) Radial velocity jumps of $\simeq 50\pm20$ km s^{-1} are observed between the bright knots at 1″ and 3.6″ and the flow just downstream (Fig. 2). Corrected for an inclination i = 42° (Dougados et al. 2000), they are compatible with shock speeds $\simeq$ 70-100 km s^{-1} derived in these features; (3) The high-velocity peak of the [O I] profile toward DG Tau has increased by 150km s^{-1} between 1984 and 1992 (Mundt et al. 1987; HEG95; SB93). A velocity variability of this amplitude could generate the strong internal shocks inferred here; (4) The wiggling of the faint jet beam section beyond 1.5″ may signal oblique shocks between the jet and its environment. Given the jet radial velocity of -280 km s^{-1}, bends of $\sim 10^\circ$ are enough to explain derived shock speeds $\simeq$ 70 km s^{-1}. The situation is somewhat reminiscent, though at higher density and 20 times smaller angular scale, of HH 46/47 where a faint, wiggling jet section with $x_{\rm e}\sim$ 0.6 (BE99) and oblique sideways shocks traced by small Hα wisps (Heathcote et al. 1996) is present between the bright inner jet and the resolved HH47A bowshock.

The presence of shocks makes it difficult to assess whether the slower, broader IV and LV flows surrounding the HV jet are intrinsic to the wind structure or whether they trace ambient material entrained by bowshock wings. Line ratios at higher spectral and spatial resolution are required to settle this issue.

Using our inferred local shock speeds and preshock densities, combined with jet radii measured from Fig. 1, we estimate the mass-flux $\dot{M}$ at various positions along the DG Tau jet using the two [O I] luminosity-based methods in Appendix A of HEG95, and the density×area-based method in Hartigan et al. (1994). While the first two methods disagree by a factor 10-100 at d =0.1-0.2″ (cf. Paper I; HEG95), all 3 give surprisingly similar, stable (within a factor of 3) values at $d > 1.2''$ of $\dot{M}\simeq$ 0.4, 0.8, and 0.2×10^{-8}M$_\odot$ yr^{-1} for the HV, IV, and LV respectively (adopting radial flow speeds of -300, -175, and -50km s^{-1} respectively, $i = 42^\circ$, and $A_V = 0$). Given an accretion rate of $\simeq 10^{-6}$ M$_\odot$ yr^{-1} (HEG95), the ejection/accretion ratio f in DG Tau must be > 0.004; it could be 100 times higher if the increase in $\dot{M}$ toward the star is real, which could be investigated by resolving the jet structure in this region.

More generally, our results for DG Tau suggest that the occurence of [N II] emission in TTS involves relatively fast shocks $\geq$ 50 km s^{-1} capable of substantially ionizing the jet. Conducting similar studies in other TTS with [N II] emission will allow to test this prediction.

Acknowledgements. We thank the OASIS team for their support during observations and data reduction, and F. Bacciotti, P. Garcia, P. Hartigan, M. Fich, A. Raga, and A. Rudolph for sharing results and discussions. C.L. was supported by a scholarship from DGAPA.

References

Bacciotti, F., Chiuderi, C., Oliva, E., 1995, A&A 296, 185
Bacciotti, F., Eislöffel, J., 1999, A&A 342, 717 (BE99)
Bacciotti, F., Eislöffel, J., Ray, T.P., 1999, A&A 350, 917
Bacon, R., et al., 2000, A&A, submitted
Binette, L., Cabrit, S., Raga, A., Canto, J., 1999, A&A 346, 260
Cabrit, S., Ferreira, J., Raga, A., 1999, A&A, 343, L61
Dougados, C., et al., 2000, submitted.
Garcia, P., et al. 2000, in preparation.
Gomez de Castro, A.I. & Pudritz, R.E. 1993, ApJ 409, 748
Hartigan, P., Morse, J.A., Raymond, J. 1994, ApJ 436, 125
Hartigan, P., Edwards, S., Gandhour, L. 1995, ApJ 452, 736 (HEG95)
Hartmann, L., Raymond, J.C., 1989, ApJ 337, 903
Heathcote, S., et al., 1996, AJ 112, 1141
Hirth, G.A., Mundt, R., Solf, J., 1997, A&AS 126, 437
Lavalley, C. et al., 1997, A&A 327, 671 (Paper I)
Mundt, R., Brugel, E.W., Buehrke, T., 1987, ApJ 319, 275
Raga, A., Böhm, K.H., Canto, J., 1996, RevMexAA 32, 161
Raymond, J.C., et al., 1994, ApJ 434, 232
Safier, P.N., 1993a, ApJ, 408, 115
Safier, P.N., 1993b, ApJ, 408, 148
Solf, J., Böhm, K.H., 1993, ApJ 410, L31 (SB93)